MAL facilitates the incorporation of exocytic uroplakin-delivering vesicles into the apical membrane of urothelial umbrella cells

Ge Zhou[a,b], Feng-Xia Liang[b], Rok Romih[c], Zefang Wang[a], Yi Liao[a], Jorge Ghiso[d], Jose L. Luque-Garcia[e], Thomas A. Neubert[b], Gert Kreibich[a], Miguel A. Alonso[f], Nicole Schaeren-Wiemers[g], and Tung-Tien Sun[a,b,h,i]

[a]Department of Cell Biology and [b]Department of Pharmacology, NYU Cancer Institute, NYU Langone Medical Center, New York University, New York, NY 10016; [c]Institute of Cell Biology, Faculty of Medicine, University of Ljubljana, 1000 Ljubljana, Slovenia; [d]Department of Pathology, NYU Cancer Institute, NYU Langone Medical Center, New York University, New York, NY 10016; [e]Department of Analytical Chemistry, Faculty of Chemical Sciences, Complutense University of Madrid, Madrid 28040, Spain; [f]Centro de Biología Molecular "Severo Ochoa," Consejo Superior de Investigaciones Científicas and Universidad Autónoma de Madrid, Madrid 28049, Spain; [g]Neurobiology Laboratory, Department of Biomedicine, University Hospital Basel, CH-4031 Basel, Switzerland; [h]Department of Dermatology and [i]Department of Urology, NYU Cancer Institute, NYU Langone Medical Center, New York University, New York, NY 10016

ABSTRACT **The apical surface of mammalian bladder urothelium is covered by large (500–1000 nm) two-dimensional (2D) crystals of hexagonally packed 16-nm uroplakin particles (urothelial plaques), which play a role in permeability barrier function and uropathogenic bacterial binding. How the uroplakin proteins are delivered to the luminal surface is unknown. We show here that myelin-and-lymphocyte protein (MAL), a 17-kDa tetraspan protein suggested to be important for the apical sorting of membrane proteins, is coexpressed with uroplakins in differentiated urothelial cell layers. MAL depletion in Madin–Darby canine kidney cells did not affect, however, the apical sorting of uroplakins, but it decreased the rate by which uroplakins were inserted into the apical surface. Moreover, MAL knockout in vivo led to the accumulation of fusiform vesicles in mouse urothelial superficial umbrella cells, whereas MAL transgenic overexpression in vivo led to enhanced exocytosis and compensatory endocytosis, resulting in the accumulation of the uroplakin-degrading multivesicular bodies. Finally, although MAL and uroplakins cofloat in detergent-resistant raft fractions, they are associated with distinct plaque and hinge membrane subdomains, respectively. These data suggest a model in which 1) MAL does not play a role in the apical sorting of uroplakins; 2) the propensity of uroplakins to polymerize forming 16-nm particles and later large 2D crystals that behave as detergent-resistant (giant) rafts may drive their apical targeting; 3) the exclusion of MAL from the expanding 2D crystals of uroplakins explains the selective association of MAL with the hinge areas in the uroplakin-delivering fusiform vesicles, as well as at the apical surface; and 4) the hinge-associated MAL may play a role in facilitating the incorporation of the exocytic uroplakin vesicles into the corresponding hinge areas of the urothelial apical surface.**

Monitoring Editor
Alpha Yap
University of Queensland

Received: Sep 29, 2011
Revised: Jan 17, 2012
Accepted: Jan 30, 2012

This article was published online ahead of print in MBoC in Press (http://www.molbiolcell.org/cgi/doi/10.1091/mbc.E11-09-0823) on February 9, 2012.

Address correspondence to: Tung-Tien Sun (sunt01@nyumc.org).

Abbreviations used: FV, fusiform vesicle; KO, knockout; MAL, myelin-and-lymphocyte protein; MDCK, Madin–Darby canine kidney cells; MVB, multivesicular bodies; OE, overexpression; siRNA, small interfering RNA; sulfo-NHS-biotin, *N*-hydroxysulfosuccinimide ester of biotin; sulfo-SHPP, *N*-sulfosuccinimidyl-3-(4-hydroxyphenyl) proprionate; TEM, transmission electron microscopy; TG, transgenic; TRE, transepithelial resistance; UP, uroplakin; Wt, wild type

INTRODUCTION

Epithelial cells perform many vectorial functions that require the polarized distribution of membrane proteins into apical and basolateral compartments, a process that has been studied extensively. Apical targeting is a two-step process: a membrane protein is first sorted at the *trans*-Golgi network (TGN) level into apical surface–destined vesicles, which are subsequently incorporated, in a regulated manner in the case of storage vesicles, into the apical surface. Very few proteins are known to play a role in directing the apical targeting of membrane proteins (Rodriguez-Boulan *et al*., 2005; Mellman and Nelson, 2008; Folsch *et al*., 2009; Carmosino *et al*., 2010b). One of them is myelin-and-lymphocyte protein (MAL;

VIP17), a 17-kDa integral membrane protein with four transmembrane domains expressed in T lymphocytes, myelin-forming cells, and many polarized epithelial cells (Alonso and Weissman, 1987; Schaeren-Wiemers *et al.*, 1995; Zacchetti *et al.*, 1995; Liebert *et al.*, 1997; Frank *et al.*, 1998; Cheong *et al.*, 1999; Marazuela *et al.*, 2003). Based largely on the in vitro data from Madin–Darby canine kidney (MDCK) cells, it has been suggested that this protein plays a key role in targeting membrane proteins to the apical surface of polarized epithelial cells (Puertollano *et al.*, 1999; Martin-Belmonte *et al.*, 2000; Rodriguez-Boulan *et al.*, 2005).

Mammalian bladder urothelium consists of basal, intermediate, and terminally differentiated, superficial umbrella cells (Khandelwal *et al.*, 2009; Wu *et al.*, 2009). The luminal membrane of the umbrella cells is almost completely covered by two-dimensional crystals of hexagonally packed 16-nm particles (urothelial plaques; Hicks and Ketterer, 1969; Vergara *et al.*, 1969; Kachar *et al.*, 1999; Min *et al.*, 2006) comprising four major integral membrane proteins—the uroplakins (UPs) Ia (26 kDa), Ib (27 kDa), II (15 kDa), and IIIa (47 kDa; Wu *et al.*, 2009). The tremendous accumulation of the uroplakin-delivering fusiform vesicles in the cytoplasm of the urothelial umbrella cells indicates that this cell type is largely dedicated to the synthesis and trafficking of the four major uroplakins. The crystalline nature of the urothelial plaques, which can be readily purified in milligram quantities (Wu *et al.*, 1990; Liang *et al.*, 2001; Min *et al.*, 2003), allows for their detailed structural analysis (Hicks and Ketterer, 1969; Vergara *et al.*, 1969; Kachar *et al.*, 1999; Min *et al.*, 2006). Such studies showed that the UPIa/II and UPIb/IIIa heterodimers are associated with the inner and outer subdomains of the 16-nm particle, respectively (Min *et al.*, 2003). Finally, the urothelial apical surface, which is accessible via a catheter, provides one of the most impressive permeability barriers known to exist in nature (Negrete *et al.*, 1996; Hu *et al.*, 2000, 2002; Kong *et al.*, 2004), and one of the uroplakins, UPIa, serves as the receptor for the type 1 fimbriated *Escherichia coli* that cause >85% of all the cases of urinary tract infections (Wu *et al.*, 1996; Zhou *et al.*, 2001; Wang *et al.*, 2009). Therefore mammalian bladder urothelium constitutes a physiologically relevant system that provides excellent opportunities for studying mechanisms of membrane trafficking.

In this work, we investigated the role of MAL in uroplakin transport, using knockout mice lacking MAL or uroplakins, transgenic mice overexpressing MAL, and MDCK cells in which MAL expression was knocked down. Our data allowed us to dissect the apical targeting of uroplakins into two phases. We conclude that MAL does not play a role in the apical sorting of uroplakins; instead, it plays an important role in facilitating the subsequent incorporation of the uroplakin vesicles into the urothelial apical membrane. Given the widespread distribution of MAL in epithelia, it is possible that these conclusions are applicable to other specialized epithelial cell types and tissues.

RESULTS

Uroplakins are targeted to the apical surface of urothelial umbrella cells

Although we showed previously that uroplakins are the major constituents of the apical surface of the umbrella cell (Wu *et al.*, 1990; Wu and Sun, 1993; Lin *et al.*, 1994; Yu *et al.*, 1994), it is unclear to what extent uroplakins are selectively targeted to the urothelial apical surface. We showed that urothelial plaques purified from mouse urothelium (Figure 1A) using sucrose density gradient centrifugation coupled with Sarkosyl wash contained four major uroplakins— uroplakins Ia, Ib, II, and IIIa (marked by filled dots in Figure 1B, lane 2; Zhou *et al.*, 2001)— plus an unknown ~18-kDa protein (Figure 1B, lane 2; open dot). In vivo biotinylation of intact mouse urothelial apical surface (Figure 1C and Supplemental Figure 1, A and B) resulted in the strong labeling of uroplakins Ia, Ib, and IIIa and weak labeling of UPII (Figure 1D), which together accounted for >80% of the total biotin label. Pretreatment of mouse urothelium with 0.1% Triton X-100 led to massive nonspecific biotinylation of cytoplasmic proteins (Supplemental Figure 1C and unpublished data), thus establishing the specificity of the surface labeling. Immuno–electron microscopy (immuno-EM) localization showed that uroplakins are exclusively associated with the luminal surface of the mouse urothelial umbrella cells, with negligible basolateral labeling (Figure 1E and inset), thus establishing that uroplakins are selectively targeted to the apical surface of mouse bladder urothelium. These data also confirmed that certain domains of the uroplakin proteins are exposed on the luminal side of the apical surface (Yu *et al.*, 1994).

MAL and uroplakin are coexpressed in upper urothelial cells

We identified the electrophoretically purified 18-kDa protein (Figure 1B, lane 7) by N-terminal sequencing as MAL (Alonso and Weissman, 1987; Schaeren-Wiemers *et al.*, 1995), a result confirmed by immunoblotting using a goat antiserum to MAL (Figure 1B, lane 9). Mouse urothelium is a stratified epithelium consisting of a basal layer of relatively undifferentiated germinative cells, one or two layers of intermediate cells, and a top layer of terminally differentiated umbrella cells (Hicks, 1975; Romih *et al.*, 2005; Khandelwal *et al.*, 2009). Immunofluorescence staining of mouse bladder sections showed that MAL and uroplakin IIIa largely coexpressed in the intermediate and umbrella cell layers (Figure 2, A and B), consistent with an earlier observation that MAL is associated with urothelial differentiation in vitro (Liebert *et al.*, 1997). High-resolution confocal microscopy revealed, however, that MAL expression preceded that of uroplakins during urothelial differentiation, as only the former was present in the apical portion of the basal cells (white downward arrows in Figure 2B). On the other hand, the apical surface of the umbrella cells, which was clearly uroplakin positive, was weakly stained by antibody to MAL (Figure 2B, 3, small arrows). Finally, confocal microscopy showed that MAL staining frequently flanked the uroplakin-positive vesicles (Figure 2, C–E).

MAL knockdown in MDCK cells has no effect on the transport of uroplakins to the apical surface but diminishes their rate of apical incorporation

To study the mechanism by which uroplakins are apically targeted, we expressed uroplakins in polarized MDCK cells. We found that singly expressed uroplakins (with the exception of UPIb) remained cytoplasmic and failed to reach the cell surface. These results are consistent with our earlier results obtained with nonpolarized 293T cells (Tu *et al.*, 2002; Hu *et al.*, 2005) and suggest that these singly expressed uroplakins were trapped in the endoplasmic reticulum (ER; Figure 3A). However, coexpression of uroplakins UPIa and Ib with UPII and IIIa, respectively, in MDCK cells allowed them to exit as UPIa/II and UPIb/IIIa heterodimers from the ER and to reach the apical cell surface (Figure 3B), colocalizing with MAL, which is known to be associated with the apical membrane (Supplemental Figure S2; Frank *et al.*, 1998; Cheong *et al.*, 1999; Puertollano and Alonso, 1999). That these uroplakin pairs became exposed on the apical surface is supported by the observations that they could be apically biotinylated (Figure 3E) and detected immunologically in intact MDCK cells (unpublished data; also see Thumbikat *et al.*, 2009). These results showed that uroplakin Ia/II and Ib/IIIa heterodimers, and even the singly expressed UPIb, harbored signals allowing them to be transported to the apical plasma membrane domain in a

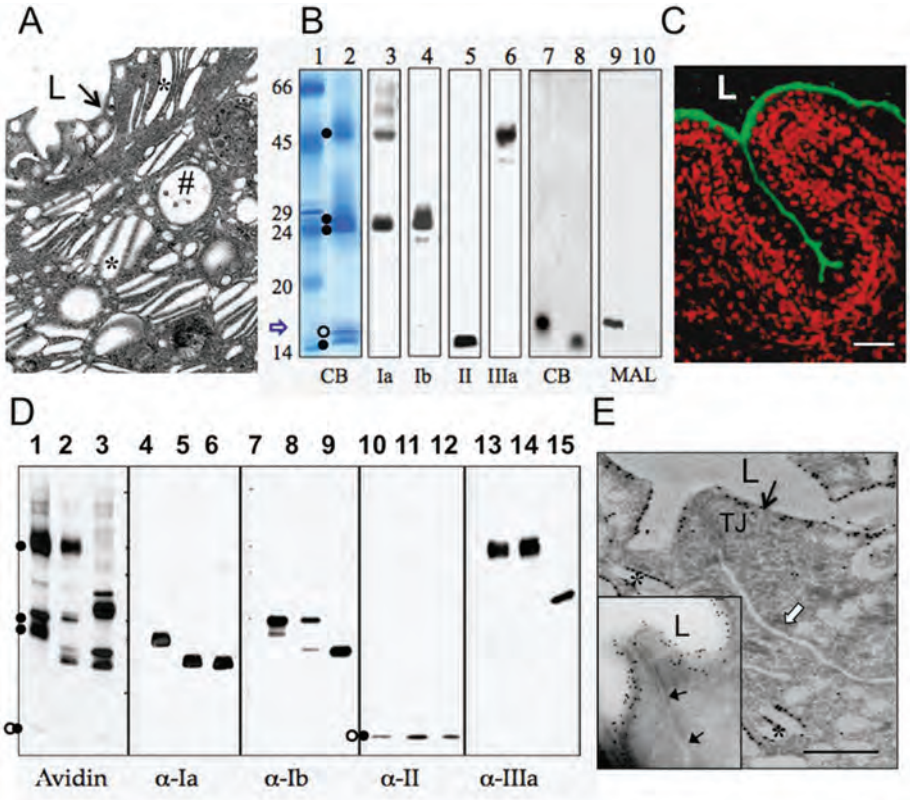

FIGURE 1: Uroplakins are apically targeted. (A) Transmission electron microscopy of a mouse urothelial umbrella cell showing the rigid-looking plaques covering the apical surface (arrow), fusiform vesicles (asterisks), and multivesicular bodies (#). (B) Identification of MAL. Lane 1, molecular weight markers. Proteins of purified mouse urothelial plaques were resolved by SDS–PAGE and stained by Coomassie brilliant blue (lane 2). The four filled dots (from the top down) denote the 47-kDa UPIIIa, 28-kDa UPIb, 27-kDa UPIa, and 15-kDa UPII, which were identified by immunoblotting using monospecific antibodies (lanes 3–6). The open dot denotes an ~18-kDa unknown protein later identified as MAL. Lane 7, electrophoretically purified 18-kDa band identified by N-terminal sequencing as MAL (see the text). Lane 8, electrophoretically purified 15-kDa UPII. Lanes 9 and 10, immunoblotting of samples shown in lanes 7 and 8 using a goat antibody to MAL. (C) Biotinylation of the mouse urothelial apical surface. Biotin was visualized using FITC-conjugated streptavidin (green fluorescence; nuclei counterstained in red). (D) The surface-biotinylated mouse bladder urothelial apical proteins are predominately uroplakins. Greater than 80% of all the biotinylated surface proteins are in the gradient-purified and Sarkosyl-insoluble uroplakin fraction. Lane 1, intact biotinylated membrane proteins, which were additionally treated with (2) Endo H and (3) Endo F. Because each uroplakin exhibits characteristic size reduction after Endo H and F treatment, these treatments, coupled with immunoblotting using monospecific antibodies to uroplakins, provide unambiguous identification of individual uroplakins. Lanes 4–15, the same three samples immunoblotted using antibodies to uroplakins Ia (lanes 4–6), UPIb (lanes 7–9), UPII (lanes 10–12), and UPIIIa (lanes 13–15). The four filled dots next to lane 1 denote, from top, UPIIIa, Ib, Ia, and II. Note that all the major biotinylated bands can be accounted for by uroplakins (Ia, Ib, and IIIa strongly and UPII weakly). (E) Immuno-EM localization of uroplakins in two neighboring (polarized) urothelial umbrella cells showing tight junction (TJ), fusiform vesicles (asterisk), apical (black downward arrow) and lateral membrane (open arrow in main panel and black arrows in inset), and lumen (L). Note the exclusive association of uroplakin-immunogold particles with the apical surface (black arrow in main panel), with none associated with the basolateral surface (open arrow). Scale bars, 1 μm (A, E) and 50 μm (C).

nonurothelial cell type, indicating that no urothelium-specific factors are required for this process.

We studied the role of MAL, which is present endogenously in MDCK cells (Puertollano *et al.*, 1999), in uroplakin delivery to the apical surface by treating the cells with small interfering RNA (siRNA; Supplemental Figure 3A). Our data indicated that the integrity of the MDCK monolayer as measured by transepithelial resistance was unaffected by the siRNA treatment (Supplemental Figure 3B) and that the siRNA-treated MDCK cells had no detectable MAL (Figure 3, C–E). Confocal microscopy showed that MAL knockdown had no effects on the basolateral distribution of the endogenous E-cadherin or the normal apical expression of the endogenous gp135 and gp114 (Figure 3F). It also had no effects on the apical delivery of the transfected uroplakin pairs UPIa/II and UPIb/IIIa (Figure 3F). To assess the role of MAL in regulating the rate of uroplakin apical incorporation, we blocked the apically exposed amino groups using sulfosuccinimidyl 3-(4-hydroxyphenyl) propionate (sulfo-SHPP), followed by biotinylating the newly exposed apical proteins either immediately (Figure 3C, lanes 1 and 2) or after 6 h (Figure 3C, lanes 3 and 4). Consistent with earlier data (Puertollano *et al.*, 1999), MAL knockdown resulted in a significant reduction in the incorporation of proteins (per 6 h) into the apical membrane. These include the endogenous proteins (~60% decrease; Figure 3C, lanes 3 and 4), as well as exogenous, transfected proteins, including hemagglutinin (Figure 3D, lanes 3 and 4; 20–30% decrease). Similar results were obtained with transfected uroplakin Ib/IIIa pair (Figure 3E, lanes 3 and 4; 60–70% reduction). These results were reproduced in three independent experiments. Given that MAL knockdown was previously shown to selectively affect MAL levels but left unaltered the content of other endogenous or exogenous proteins analyzed (Cheong *et al.*, 1999; Puertollano *et al.*, 1999; Martin-Belmonte *et al.*, 2000, 2001), it is unlikely that the observed alterations were due to changes in the total content of hemagglutinin or UPIIIa. Taken together, these data indicated that MAL knockdown had no effect on the total content of apical uroplakins (Figure 3F) but significantly reduced the rate of uroplakin incorporation into the apical membrane (Figure 3E).

Deficiency or overexpression of MAL in vivo has no effect on the apical association of uroplakins

To study the functional roles of MAL in vivo in uroplakin trafficking, we studied uroplakin delivery to the umbrella cell plasma membrane in MAL-knockout mice (Schaeren-Wiemers *et al.*, 2004), whose urothelium, as expected, had no detectable MAL message or protein (Figure 4, A–C). Consistent with the results in MAL-knockdown MDCK cells (Figure 3F), the apical distribution of uroplakins was unaffected (Figure 4, D–F). Parallel analyses of the MAL-overexpressing mouse urothelium (Frank *et al.*, 2000) indicated that it had an elevated (threefold to fivefold) level of MAL message and protein (Figure 4, A–C). Immuno-EM localization showed, again, the exclusive association of

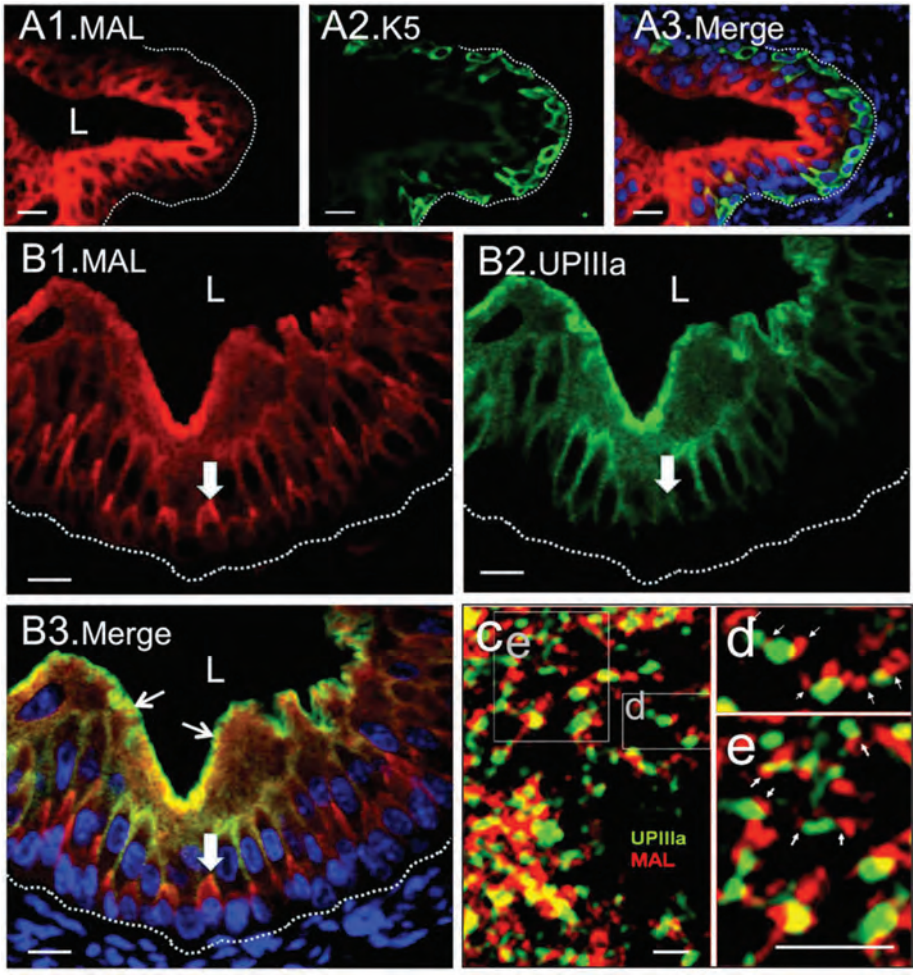

FIGURE 2: MAL expression precedes that of uroplakins during urothelial differentiation. (A) A section of mouse bladder was double immunostained using a goat antibody to MAL (red) and a mouse antibody to a basal cell keratin K5 (green); note the progressive increase in MAL staining intensity in the upper cell layers. (B) Double immunostaining of a mouse bladder section with a goat anti-MAL (red) and a mouse monoclonal antibody to uroplakin IIIa (green); note in the merged image that MAL can be detected in the top portion of basal cells (white arrow), which is uroplakin negative, and that the apical surface of the umbrella cells is uroplakin positive but MAL weak (green; arrows in B3; cf. Figure 6, F and G). (C) A high-resolution image of a small zone in an umbrella cell localizing MAL (red) and UPIIIa (green). (D, E). Enlargement of the two boxed areas in C. Note that in many cases MAL (arrows) flanks the uroplakin vesicle–like structures. Bars, 10 μm (A, B) and 0.5 μm (C, E).

uroplakins with the apical surface, with no basolateral association (Figure 4, G–I). These results indicated that varying the in vivo MAL level from zero (in the case of gene knockout) to threefold to fivefold higher than normal (transgenic) had no detectable effects on the apical association of uroplakins, suggesting that MAL played no role in the sorting of uroplakins into fusiform vesicles that are targeted to the apical plasma membrane domain in mouse urothelial umbrella cells.

MAL affects the rate by which uroplakins are delivered to the apical surface and its subsequent endocytic degradation

Although MAL knockout had no effects on the level of uroplakin messages (Figure 4A), it led to a 3- to 10-fold increase in uroplakin protein content per cell (Figure 4B) and a significant accumulation of the uroplakin-delivering fusiform vesicles (Figure 5, C–E). MAL overexpression also had no effects on the uroplakin message level but led to a 5- to 8-fold decrease in uroplakin content (Figure 4B) and a partial replacement of the fusiform vesicles by multivesicular vesicles (which are lined with uroplakin-positive plaques; Figure 5, F–H; and unpublished data). These results are in complete agreement with our MDCK cell data (Figure 3, C and D) and suggest that MAL depletion retards the apical incorporation of uroplakins. These data also indicate that MAL plays an important role in determining the steady-state status of the uroplakins, that is, whether the uroplakins exist mainly in fusiform vesicles (of the exocytic/biogenetic pathway) or the multivesicular vesicles (of the endocytic/degradative pathway).

MAL is associated with the hinge areas of the uroplakin-delivering vesicles

To determine the spatial relationship between MAL and uroplakin, we localized MAL and uroplakins in mouse urothelial umbrella cells (Figure 6A) by immuno-EM. Whereas uroplakins were associated with the two plaques in a fusiform vesicle (Figure 4, D and G; Figure 6E; also see Liang *et al.*, 2001), MAL was found to be associated with the uroplakin-free hinge areas (Figure 6, B–E). In the apical surface, which also contained uroplakin plaques interconnected by hinge areas, MAL was again associated with the hinges (Figure 6F). The association of MAL with the hinges of the apical surface could be seen more clearly in the MAL-overexpressing bladder urothelium (Figure 6G). MAL was also detected at the hinges of the multivesicular bodies (unpublished data). These results indicate that even though MAL and uroplakins coexist in the same fusiform vesicles, they are associated with distinct membrane subdomains.

Uroplakin knockout leads to the accumulation of small, MAL-containing vesicles

To assess the effects of removing the uroplakin cargoes from the exocytic fusiform vesicles, we examined the urothelium of uroplakin-knockout mice (Hu *et al.*, 2000; Kong *et al.*, 2004). Electron microscopy showed that uroplakin depletion led to the complete replacement of the fusiform vesicles by numerous rounded vesicles that were 200–300 nm in diameter (Figure 7, A–C; Hu *et al.*, 2002; Kong *et al.*, 2004). Immunofluorescence staining and immuno-EM localization data showed that these uroplakin-depleted vesicles were MAL positive (Figure 7D) and accumulated toward the subapical zone (Figure 7, B, D and E).

MAL and uroplakins are associated with lipid rafts

MAL has been shown to be lipid raft associated in MDCK and Fischer rat thyroid FRT cells (Zacchetti *et al.*, 1995; Martin-Belmonte *et al.*, 1998, 2001), and this has been proposed to be a mechanism for MAL-mediated sorting of proteins to the apical surface of epithelial cells (Cheong *et al.*, 1999; Puertollano *et al.*, 1999; Martin-Belmonte *et al.*, 2000). To see whether MAL and uroplakins are raft associated in mouse urothelial cells, we prepared an extract of the

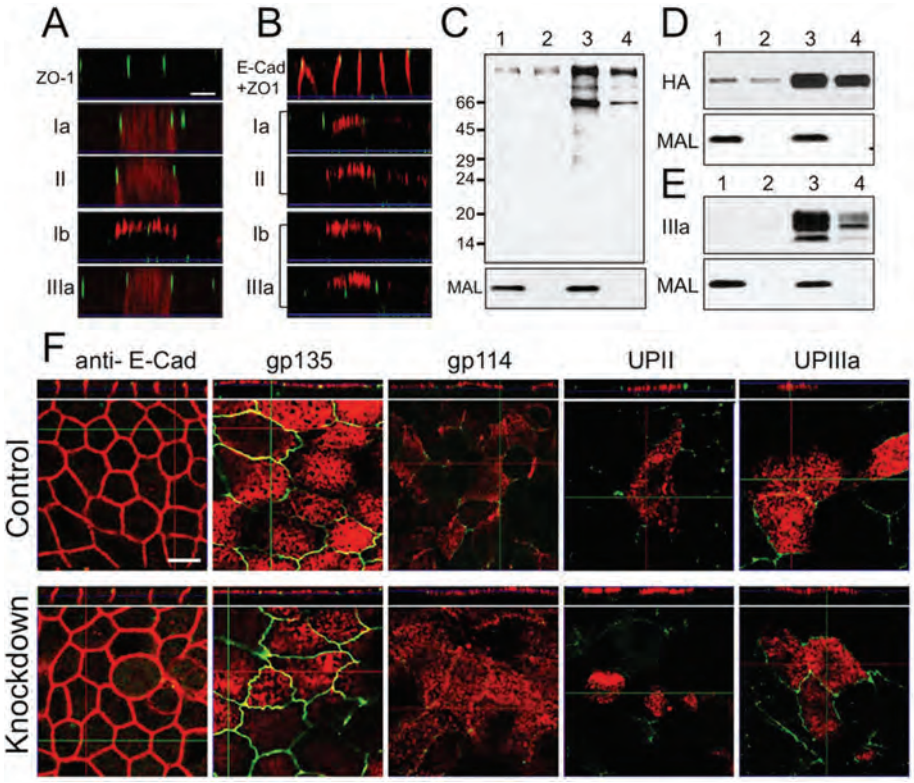

FIGURE 3: Depletion of MAL in MDCK cells does not affect the apical sorting of uroplakins, but it reduces their rate of apical incorporation. (A) Individual uroplakins (except UPIb) expressed alone in MDCK cells fail to reach the apical surface. MDCK cells transfected with uroplakin Ia, II, Ib, and IIIa were fixed at 36 h posttransfection, permeabilized with 0.5% Triton X-100 at 25°C for 10 min, double stained with rabbit antibodies to the indicated uroplakins (red) and a rat monoclonal antibody to the ZO1 tight junction apical marker (green), and observed by confocal microscopy. (B) Uroplakins expressed as a UPIa/UPII or UPIb/UPIIIa pair (brackets) can reach the apical surface. Top, the localization of ZO-1 (green) and E-cadherin (red) as markers for the apical boundary and basolateral membrane. (C) siRNA knockdown of the MAL reduces the delivery rate of apical proteins. MDCK cells were transfected with a control (scrambled; odd-numbered lanes) or a double-stranded siRNA (siRNA200; even numbered) that knocked down the endogenous dog MAL expression (Supplemental Figure S3), seeded into a Transwell, and incubated at 37°C for 36 h. The free amino groups exposed on the apical cell surface were blocked by applying a solution of sulfo-SHPP to the apical compartment of the Transwell, and the newly arrived apical surface proteins were tagged by sulfo-NHS-biotin either immediately (lanes 1 and 2) or after 6 h at 37°C (lanes 3 and 4). Newly exposed apical surface proteins were detected, after SDS–PAGE, using peroxidase-labeled streptavidin (top), and MAL was detected using an anti-MAL antibody (bottom). Note the efficient depletion of MAL expression and the ~60% reduction in the apical delivery of endogenous surface proteins. (D, E) MAL depletion reduces the apical incorporation rate of hemagglutinin (HA) and uroplakins. MDCK cells were transfected with control scrambled siRNA (single-numbered lanes) or si200 RNA (even numbered) and (D) infected with influenza virus or (E) transfected with cDNAs encoding the UPIb/UPIIIa uroplakin pair. Newly appearing apical surface proteins were biotin tagged as described in C either immediately (lanes 1 and 2) or after 6 h (lanes 3 and 4). These biotin-tagged apical proteins were affinity pulled down using streptavidin beads and blotted using antibodies to HA (D) or UPIIIa (E). Note that MAL depletion led to ~20–30% decrease in the apical delivery of HA and ~60–70% in that of UPIIIa. Similar results were obtained in three independent experiments. (F) MAL depletion had no effect on the apical distribution of uroplakins, gp135, and gp114. MDCK cells were transfected with control siRNA (top, Control) or Si200 (bottom, Knockdown) and were transfected 36 h later with cDNAs encoding UPIa/II or UPIb/IIIa. The transfected cells were grown for 36 h, fixed, Triton permeabilized, and immuno-stained for E-cadherin (an endogenous basolateral marker), gp135, and gp114 (both endogenous apical markers), uroplakin II (for the UPIa/II cotransfection), or uroplakin Ib (for UPIb/IIIa) and visualized by confocal microscopy. Top, *x-z* images of a vertical section. Bottom, *x-y* plane (projected *z*-series). Note that MAL depletion had no effect on the apical targeting of uroplakins II and IIIa, gp135, and gp114. Bar, 10 μm.

total mouse urothelial membrane proteins in 0.5% Triton X-100. After centrifugation to equilibrium in a discontinuous sucrose density gradient, the protein fractions were analyzed by silver staining and immunoblotting (Figure 7, F and G). The results indicated that some of the uroplakins (~20%) floated in a low-density fraction (lanes 8 and 9 in Figure 7, F and G) that corresponded to the interface between the 37 and 5% sucrose (Duncan *et al.*, 2004; Khandelwal *et al.*, 2010). Moreover, we found that almost all of the MAL (>80%) cofloated with the uroplakins, suggesting that under these experimental conditions both MAL and uroplakins are associated with Triton X-100–insoluble lipid-raft fractions (Figure 7, F and G).

DISCUSSION

MAL does not play a role in the sorting of uroplakins to the apical surface

Our biotinylation (Figure 1, C and D) and immuno-EM localization data (Figure 1E) established that uroplakins are major integral membrane protein components of the urothelial luminal surface and that uroplakins are apically targeted. Transfection studies of MDCK cells show that the formation of correct uroplakin pairs (UPIa/UPII and UPIb/UPIIIa) is a prerequisite for their ER-exit *and* apical delivery (Figure 3B; with the exception of UPIb, which can exit alone—see Figure 3A). Although these pair-formation data are consistent with our earlier observations made in the nonpolarized 293T cells (Tu *et al.*, 2002; Hu *et al.*, 2005, 2008), the use of polarized MDCK cells here enabled us to demonstrate for the first time that uroplakins can be sorted to the apical membrane in a nonurothelial cell type, thus proving that these proteins must harbor intrinsic signals for apical delivery, without the need for urothelium-specific factors. Finally, we demonstrated that MAL depletion, in MDCK cells (Figure 3) as well as in vivo in the urothelium of the MAL-knockout mice (Figure 4), had no effect on the transport of uroplakins to the apical domain, indicating that MAL is not required for the apical sorting of these membrane proteins.

MAL facilitates the incorporation of the fusiform vesicles into the apical urothelial membrane

Our data indicate that although MAL is dispensable for the sorting of uroplakins into apically destined fusiform vesicles, it plays a role in the incorporation of these exocytic uroplakin-delivering vesicles into the apical surface. First, knockdown of MAL in MDCK cells reduced the rate by which uroplakins (Figure 3E), hemagglutinin (Figure 3D), and

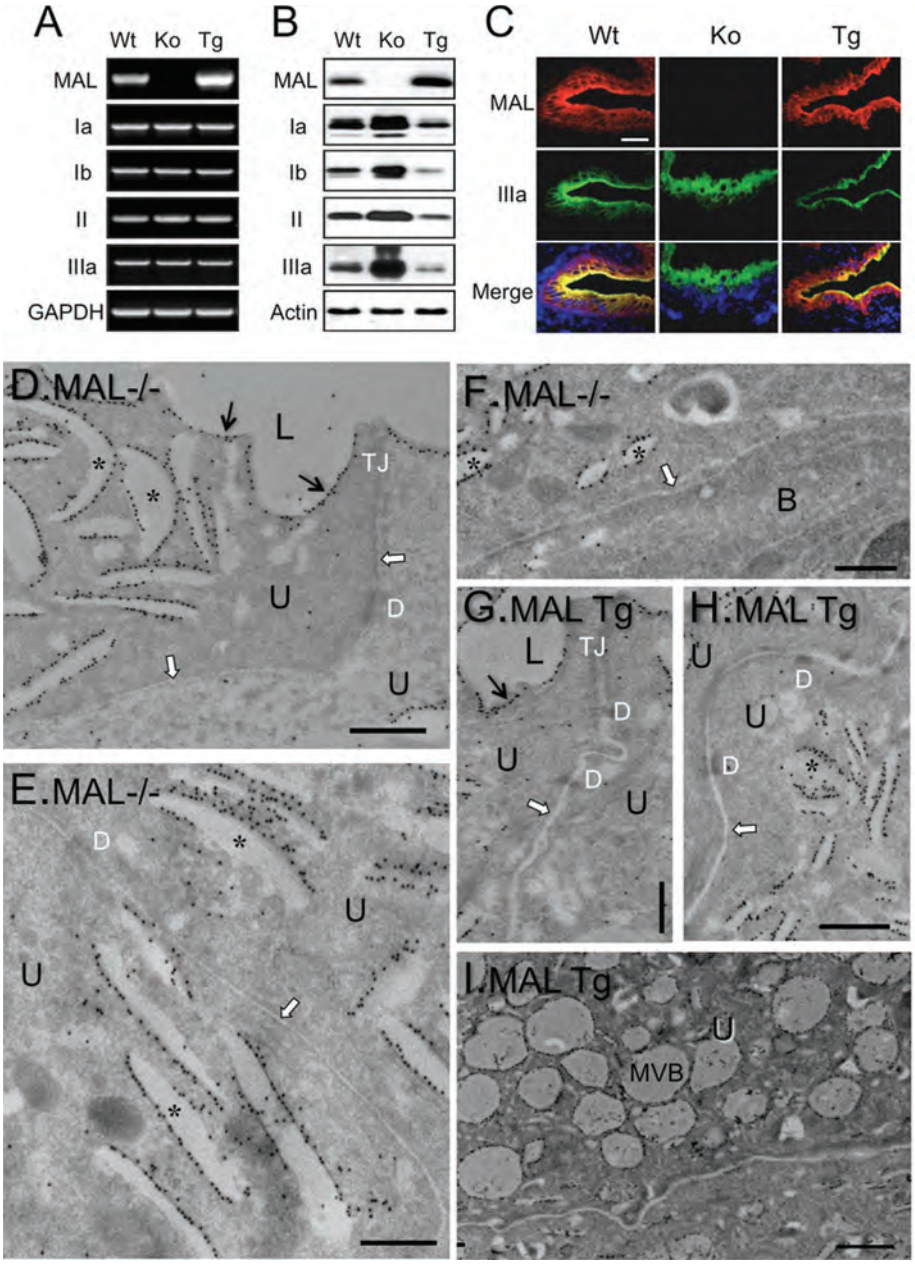

FIGURE 4: Genetic ablation and overexpression of MAL did not affect the transport of uroplakins to the apical plasma membrane of mouse urothelial umbrella cells. (A) RT-PCR analyses. Total RNA from the urothelia of wild-type (Wt), Ko (MAL knockout). and Tg (MAL transgenic/overexpressing) mouse bladder were subjected to RT-PCR analyses using primers for, as indicated, MAL, uroplakins Ia, Ib, II, and IIIa, and glyceraldehyde-3-phosphate dehydrogenase (GAPDH; as a loading control). Note the absence and 3- to 5-fold increase in MAL messenger in the Ko and Tg samples, respectively, and the relatively constant level of uroplakin mRNAs. (B) Western blot analyses. Total proteins of Wt, Ko, and Tg bladder urothelium were resolved by SDS–PAGE, transferred onto a nitrocellulose membrane, and reacted with antibodies to MAL, uroplakins Ia, Ib, II, and IIIa, and actin (loading control). Note that the Ko urothelium contained no MAL and a 3- to 10-fold increase in uroplakin contents, whereas the Tg urothelium contained a 3- to 4-fold increase in MAL but a 5- to 8-fold decrease in uroplakins. (C) Immunofluorescence staining. Paraffin-sections of Wt, Ko, and Tg mouse bladder were double immunostained for MAL (red) and uroplakin IIIa (green). Bar, 20 μm. Note that the uroplakin staining intensities increased significantly in Ko but decreased in Tg. (D–I) Immuno-EM localization of uroplakins in (D–F) MAL-knockout urothelial cells and (G–I) MAL-overexpressing urothelial cells. Note in D–F that MAL knockout did not affect the formation of the uroplakin-delivering fusiform vesicles (asterisks), did not prevent the apical expression of uroplakins (black arrows in D), and did not result in the mistargeting of the uroplakins to the basolateral surface (open arrows in D–F). Also note that MAL overexpression (G–I) did not affect the apical distribution of uroplakins (black arrow in G) and led to the formation of numerous multivesicular bodies (I; also see Figure 5). asterisk, fusiform vesicle; D, desmosome; I, intermediate cell; L, lumen; MVB, multivesicular body; TJ, tight junction; U, umbrella cell. Bars, 50 μm (C) and 0.5 μm (all others).

many other endogenous proteins (Puertollano *et al.*, 1999; Martin-Belmonte *et al.*, 2000; Figure 3C) appeared on the apical surface. Second, ablation of the mouse MAL gene led to the accumulation of fusiform vesicles (Figure 5D) and an increase in the cellular uroplakin content (Figure 4B), suggesting a partial blockage of the incorporation of the uroplakin-delivering vesicles into the luminal surface (Figure 8B). Third, MAL overexpression led to the partial replacement of fusiform vesicles by multivesicular bodies (Figure 5, F–H), suggesting enhanced exocytosis and compensatory endocytosis (Figure 8C; Truschel *et al.*, 2002; Gundelfinger *et al.*, 2003; Vogel, 2009; Khandelwal *et al.*, 2010). This interpretation is consistent with the fact that the multivesicular bodies of urothelial umbrella cells are often lined with uroplakin plaques, suggesting their involvement in the recycling (Back *et al.*, 2010) or, more likely, lysosomal degradation of uroplakins (Amano *et al.*, 1991; Khandelwal *et al.*, 2010). Finally, EM localization data showed that MAL could reach the urothelial apical surface (Figure 6, F and G). This interpretation is consistent with our observation that, although MAL was not significantly surface-biotinylated in mouse urothelium (Figure 1D), it was heavily labeled in bovine urothelium (unpublished data). It is also consistent with the finding that MAL can reach the apical surface of MDCK cells (Supplemental Figure S2; Puertollano and Alonso, 1999) and can be recycled to the TGN, suggesting that MAL is an itinerant protein cycling between the TGN and the plasma membrane (Puertollano and Alonso, 1999). Taken together, these data indicate that MAL plays a critical role in the efficient incorporation of the exocytic uroplakin-delivering vesicles into the urothelial apical membrane.

Thus our data indicate that MAL does not play a role in the apical sorting of uroplakins, gp114, and gp135 and the faithful incorporation of uroplakins into fusiform vesicles that can fuse with the apical surface of umbrella cells (Figure 3F). Our gp114 result is apparently inconsistent with an early report that this protein was mistargeted to the basolateral membrane in MAL-depleted MDCK cells (Cheong *et al.*, 1999); the reason

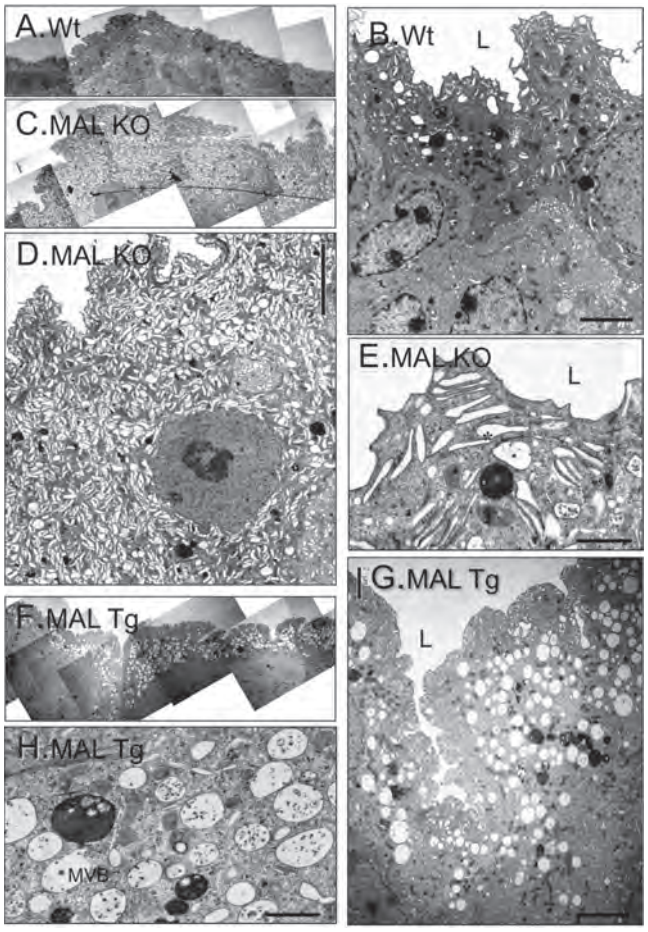

FIGURE 5: MAL knockout resulted in an accumulation of fusiform vesicles, whereas MAL overexpression led to the partial replacement of fusiform vesicles by multivesicular bodies. Transmission electron microscopy of the wild-type (A, B), MAL-knockout (C–E), and MAL-overexpressed (F–H) mouse bladder urothelium. Note in C–E the accumulation of the uroplakin-delivering fusiform vesicles and in F–H the partial replacement of the fusiform vesicles by the degradative multivesicular vesicles. Bars, 10 μm (B, D, G) and 2 μm (E, H).

for this discrepancy is unclear. In sum, our MDCK and in vivo data are consistent with each other and strongly suggest that the main in vivo function of MAL in mouse urothelial umbrella cells is to facilitate the incorporation of exocytic vesicles into the apical surface membrane, after they have been tethered to the apical zone by a MAL-independent mechanism. Additional studies are needed to determine whether MAL, a compact, highly hydrophobic, four-transmembrane-domain membrane protein (Magal *et al.*, 2009), may function as one of the effectors that embed and regulate the soluble *N*-ethylmaleimide–sensitive factor attachment protein receptor–Sec1/Munc18-like or other related fusion machinery (Sudhof and Rothman, 2009).

Possible mechanisms for the apical targeting of uroplakins

Existing data suggest that apical sorting may be facilitated by the coalescence of nanoscale assemblies of lipid rafts into larger, stabilized platforms that can function in signal transduction and membrane trafficking, and that this coalescence process may be promoted by caveolin oligomers, luminal lectins, and other apical sorting receptors (Fullekrug and Simons, 2004; Rodriguez-Boulan *et al.*, 2005; Vagin *et al.*, 2009; Simons and Gerl, 2010). This process has also been shown to be facilitated by protein oligomerization (Paladino *et al.*, 2004, 2007). Our finding that some of the uroplakins are associated with lipid rafts (Figure 7, F and G; Khandelwal *et al.*, 2010), coupled with the strong propensity of uroplakins to polymerize forming heterodimers, heterotetramers,16-nm particles, and two-dimensional (2D) crystals (Tu *et al.*, 2002; Hu *et al.*, 2005, 2008), suggests that these may provide dominant signals for the apical sorting of uroplakins, although Rab27b (Chen *et al.*, 2003) and Rab11a (Khandelwal *et al.*, 2008) may also contribute to or modulate this process.

It is interesting that in the absence of MAL expression uroplakins can still form normal-looking fusiform vesicles, indicating that MAL is not required for fusiform vesicle formation. However, these MAL-negative vesicles seem to be less efficient in fusing with the apical membrane (Figure 5, D and E; also see Figure 3E). This result contrasts with the case of some other apical proteins examined so far, which, when MAL was depleted, become retained in the Golgi (Cheong *et al.*, 1999; Martin-Belmonte *et al.*, 2001). MAL therefore appears to facilitate the delivery of the transport vesicles at the TGN level for some type of cargoes, but it functions only in the final stage of apical incorporation of the uroplakin storage vesicles.

The strong propensity for the uroplakins to polymerize forming 2D crystals even at an early stage of assembly leads to the clean separation of uroplakins and MAL into the plaque and hinge areas of the fusiform vesicle, respectively (Figure 6A). This suggests that MAL may not interact directly with uroplakins and that it is unlikely that uroplakin–MAL interaction per se plays a role in the apical sorting of uroplakins (cf. Tall *et al.*, 2003).

The formation of membrane subdomains has been implicated in signal transduction and membrane trafficking. However, these subdomains are usually quite small and heterogeneous, exhibiting a spectrum of lipid and protein composition and properties, thus complicating their study (Jacobson *et al.*, 2007; Coskun and Simons, 2010; Lingwood and Simons, 2010). For example, tetraspanins (to which uroplakins Ia and Ib belong) form membrane microdomains that are distinguishable from typical "rafts" in their detergent resistance and protein composition (Hemler, 2003; Wright *et al.*, 2004; Le Naour *et al.*, 2006; Lazo, 2007; Yanez-Mo *et al.*, 2009). Uroplakin proteins are exceptional in that they form huge, well-characterized membrane subdomains that can reach 500–1000 nm in diameter, in this case forming 2D crystalline plaques with well-defined protein and probably lipid composition (Lingwood and Simons, 2010; Simons and Gerl, 2010).

Roles of MAL in regulating the apical delivery of uroplakins in the polarized urothelial umbrella cells: a model

Taken together, our data suggest a model in which MAL is an integral part of a class of exocytic vesicle that transports the uroplakin cargoes to the apical surface of mouse urothelium (Figure 8). This model has the following salient features:

1) Normal mouse urothelial umbrella cells (Figure 8A). In this case, the newly synthesized uroplakins are probably enriched in the MAL (green arrowheads)–containing lipid raft subdomains of the TGN. These uroplakin/MAL subdomains are pinched off, forming uroplakin-delivering, immature discoidal vesicles containing scattered or loosely aggregated uroplakin particles (Severs and Hicks, 1979; Hudoklin *et al.*, 2011). Homotypic fusion and retrograde transport of the nonuroplakin domains lead to the expansion of the 2D crystals of uroplakins and progressive decrease of the MAL-to-uroplakin ratio, culminating in the formation of a mature fusiform vesicle consisting of two large 2D crystals of uroplakins interconnected by MAL-positive, uroplakin particle–free hinge

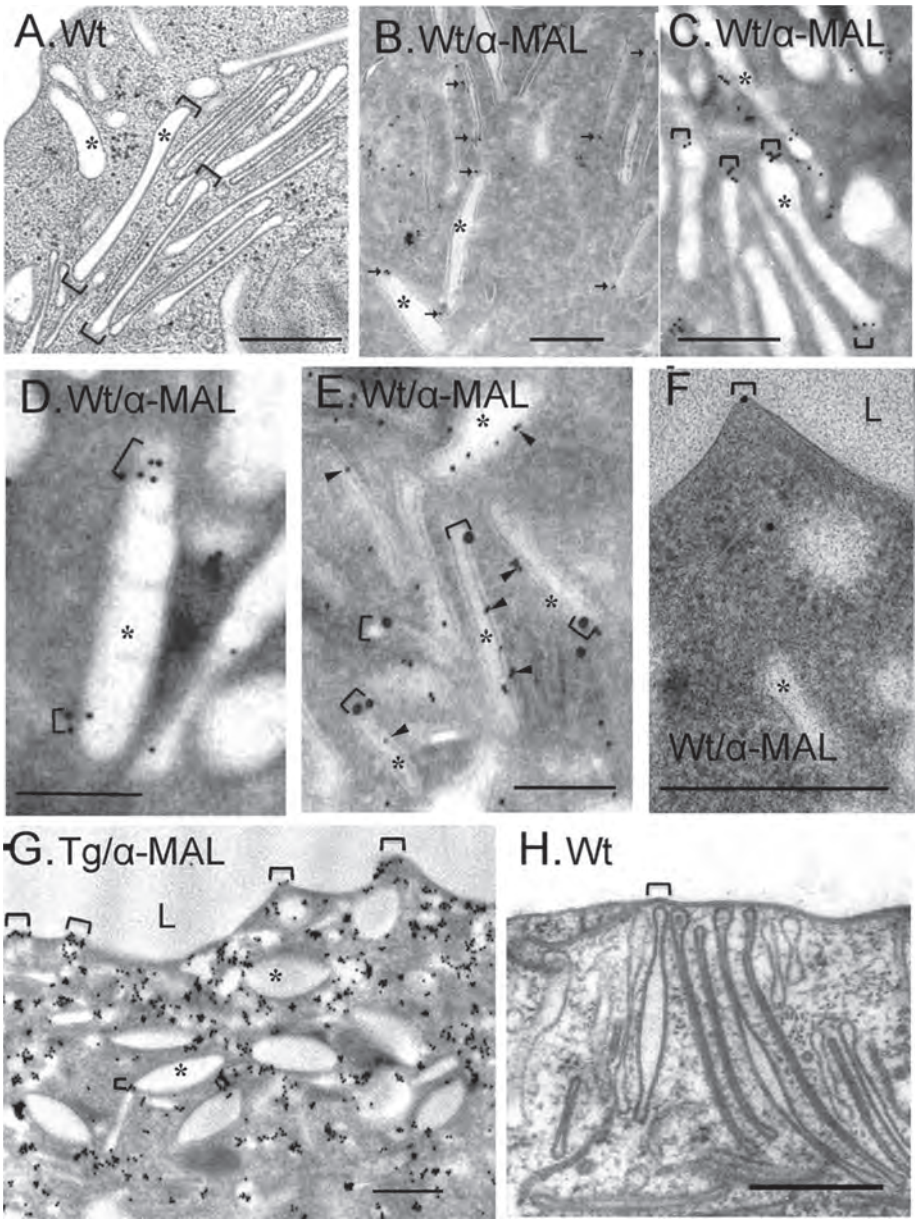

FIGURE 6: MAL is associated with the hinge areas of the fusiform vesicles and the apical surface of mouse urothelium. (A) Ultrastructure of a Wt mouse urothelial umbrella cell showing that a fusiform vesicle (asterisk) consists of two large uroplakin plaques interconnected by hinge areas (brackets). (B–F) EM immunogold labeling of MAL using a goat anti-MAL antibody (*Materials and Methods*), with E showing double immuno-EM localization of MAL (15-nm gold particles; brackets) and uroplakins (6-nm; arrowheads). (H) Apical surface of mouse urothelial umbrella cell showing an area (bracketed) where the hinge areas of several fusiform vesicles are in proximity with a hinge of the apical surface. Note that MAL (arrows in B and brackets in C–G) is mainly associated with the hinges of the fusiform vesicles and the apical surface (F, G). Bars, 1 μm (F) and 0.5 μm (all others).

areas (Figures 1A and 6, A and H; Kachar *et al.*, 1999; Liang *et al.*, 1999). This hypothesized sequence is based on the following considerations:

a) The small, MAL-positive vesicles in the umbrella cells of the uroplakin-knockout mouse urothelium. Our data indicate that genetic ablation of uroplakins, the main cargo of the MAL-containing vesicles, blocked the formation of fusiform vesicles, leading to the accumulation of numerous, empty-looking MAL-positive spherical vesicles (Figure 7, B–E). Immunoblotting analysis of these vesicles, which are enriched in a Sarkosyl-insoluble fraction, confirmed the presence of a large amount of MAL (unpublished data). These data suggest that the small vesicles in uroplakin-deficient urothelial cells (Figure 7, B–E) are similar to the early discoidal vesicles without their uroplakin cargo and that MAL is an integral protein component of the uroplakin-delivering vesicles in normal umbrella cells (Figure 7, B–E).

b) Segregation of MAL from the uroplakins. Although MAL is relatively uniformly distributed in the immature discoidal vesicles (Figure 7, D and E), it is progressively excluded from the expanding 2D crystals of uroplakins, so that in mature fusiform vesicles it is associated exclusively with the uroplakin-free hinge areas (Figure 6, B–E). MAL is also associated with the hinge areas of the apical surface membrane (Figure 6, F and G). The fact that the plaque-associated hinge areas, like the plaques, can survive detergent treatment (Liang *et al.*, 2001) explains why MAL copurified (Figure 1B) and cofloated (Figure 7, F and G) with uroplakins.

c) Hinge area as a possible site of fusion. The fact that MAL is associated with the (uroplakin particle–free) hinge areas of not only the fusiform vesicles (Figure 6, B–E) but also those of the apical surface (Figure 6, F and G) raises the possibility that the MAL-enriched hinge areas are involved in the fusion between the fusiform vesicles and the urothelial apical surface (Figure 6H). The mechanism by which MAL facilitates the fusion of the exocytic vesicle with the apical membrane is unclear, but it may involve a MAL and related proteins for vesicle trafficking and membrane link (MARVEL) domain, which is found in MAL, physins, gyrins, and occludin families (Sanchez-Pulido *et al.*, 2002). These MARVEL-containing proteins may function in cholesterol-rich membrane opposition events in a variety of cellular processes (Sanchez-Pulido *et al.*, 2002). The accumulation of fusiform vesicles in urothelial cells from MAL-knockout mice is reminiscent of that of prefusion complexes in mutants of the MARVEL domain–containing Singles Bar protein, which is required for the prefusion complex of myoblasts to progress to fusion in *Drosophila* embryos (Estrada *et al.*, 2007).

d) The uroplakin-delivering fusiform vesicles can be regarded as a form of storage vesicles whose fusion with the apical surface may be up-regulated by the mechanical distention of the bladder (Lewis and de Moura, 1982; Truschel *et al.*, 2002; Khandelwal *et al.*, 2009; Wu *et al.*, 2009).

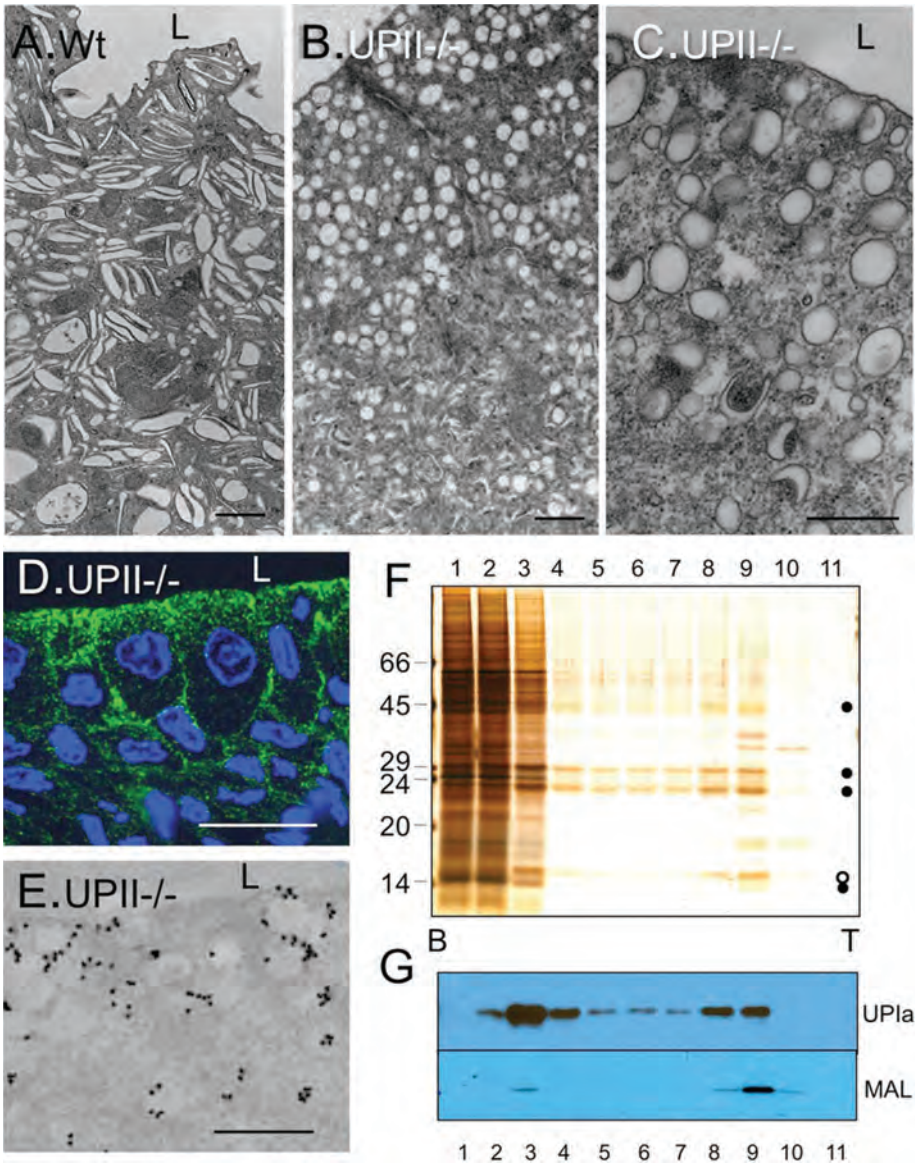

FIGURE 7: MAL is associated with the small vesicles in the uroplakin-depleted mouse urothelium and is raft associated. (A–C) Ultrastructure of the bladder urothelial umbrella cells of (A) Wt or (B, C) a UPII-knockout (UPII$^{-/-}$) mouse (Kong *et al.*, 2004), showing that uroplakin knockout led to the replacement of fusiform vesicles (500–800 nm) by round vesicles (~200–nm). (D) Immunofluorescence staining of MAL in a section of the uroplakin II–knockout mouse urothelium showing the accumulation of MAL-positive vesicles toward the apical zone. (E) Immuno-EM localization showing the presence of MAL in these small vesicles. Bars, 0.5 μm (A–C and E) and 20 μm (D). (F, G) Total mouse urothelial membrane proteins were suspended in a lysis buffer containing 0.5% Triton X-100 and 55% sucrose (see *Materials and Methods*) and subjected to centrifugation to equilibrium in a discontinuous sucrose density gradient. After fractionation, the proteins of each fraction were analyzed by SDS–PAGE and silver nitrate staining (F) or immunoblotting using antibodies to uroplakin Ia or MAL (G). The four black dots on the right of lane 11 mark the position of, from the top, uroplakin IIIa, Ib, Ia, and II (molecular weight 47, 28, 27, and 15 kDa, respectively), and the open dot marks the position of MAL (18 kDa). B and T denote the bottom and top of the gradient, respectively. Note that >80% of the MAL exists in a light, Triton X–100-resistant "raft" fraction that also contained uroplakins.

e) Uroplakin/MAL endocytosis. The uroplakins that are associated with the apical surface undergo endocytosis in an clathrin- and caveolin-independent manner (Khandelwal *et al.*, 2010), and are delivered to early endosomes, which are then delivered to multivesicular vesicles and lysosome (for degradation (Figure 5, F and H). One cannot rule out the possibility, however, that some of the endocytosed uroplakins can be recycled (hence the question marks in Figure 8A).

2) MAL-depleted urothelial cells (Figure 8B). Because the MAL-depleted urothelial umbrella cells can still make fusiform vesicles and the apical surface of such cells is covered by uroplakin plaques (Figure 5, D and E), MAL is clearly *not* required for fusiform vesicle formation and for their incorporation into the apical surface. However, MAL facilitates the fusion of the exocytic vesicles with epithelial apical surface, so that even though in its absence this fusion can still occur, it proceeds with a lower rate (Figure 3E), leading to the accumulation of fusiform vesicles (Figure 5, D and E; highlighted in a dashed circle in Figure 8B) and an increase in uroplakin content (Figure 4, A and B).

3) MAL-overexpressing urothelial cells (Figure 8C). MAL overexpression facilitates the apical incorporation, and subsequent endocytic degradation, of uroplakins, thus explaining the observed decrease in fusiform vesicles, accumulation of the multivesicular bodies (Figure 5, G and H; highlighted in a dashed circle in Figure 8C), and decreased uroplakin content (Figure 4, A and B).

Concluding remarks

Our results enabled us to dissect the apical targeting of uroplakins into two phases—the apical sorting process at the TGN level and the final incorporation of the apically targeted, uroplakin-delivering vesicles into the apical surface. We showed that MAL does not play a role in the apical sorting of uroplakins at the TGN level. Instead, it plays an important role in facilitating the subsequent incorporation of the uroplakin-delivering exocytic vesicles into the urothelial apical membrane. Although our data are based on urothelium and cultured MDCK renal cells, MAL is present near or on the apical surface of a wide range of polarized epithelial cells, including those of the respiratory, gastrointestinal, and genitourinary tracts, and in exocrine and endocrine glands such as thyroid and pancreas (Marazuela *et al.*, 2003). In addition, MAL overexpression can lead to abnormal apical membrane formation in cultured thyroid cells (Martin-Belmonte *et al.*, 1998, 2000) and in kidney and stomach epithelia in transgenic mice (Frank *et al.*, 2000; Carmosino *et al.*, 2010a). These results raise the possibility that MAL may play a similar role in facilitating the incorporation of exocytic vesicle into the apical surface of a wide range of specialized epithelial cells.

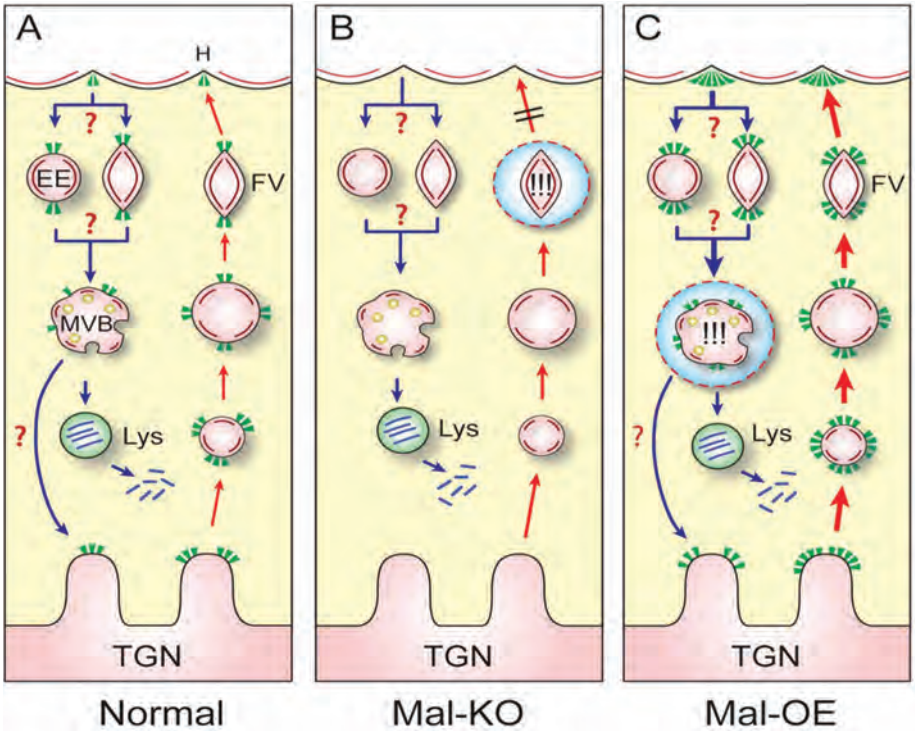

FIGURE 8: A model showing the in vivo function of MAL in mouse bladder urothelium, facilitating the apical delivery of uroplakins. (A) In normal mouse urothelial umbrella cells, MAL (green triangles representing only the cytoplasmic domains of this tetraspan protein) is enriched in raft subdomains in TGN and early discoidal vesicles. It is excluded by the expanding uroplakin 2D crystals, ending up in the uroplakin-free hinge areas of the mature fusiform vesicles (FVs) and the apical membrane. MAL and uroplakins can be retrieved from the apical surface as early endosomes (EEs), which go through multivesicular bodies (MVBs) and lysosomes (Lys) for degradation. The possibility of endocytosed uroplakins becoming fusiform vesicles is unlikely but cannot be completely ruled out (question mark). (B) In the absence of MAL (as in the umbrella cells of the MAL-knockout mouse), the incorporation of fusiform vesicles to the apical surface can still occur but at a lower rate, resulting in the accumulation of FV (dashed circle). (C) When MAL is overexpressed (as in the case of MAL transgenic), most of the fusiform vesicles fuse with the apical surface, thus enhancing compensatory endocytosis (Vogel, 2009; Khandelwal *et al.*, 2010) and the accumulation of multivesicular bodies (in dashed circle). See the text for details.

MATERIALS AND METHODS

Antibodies and tissues

Rabbit antiserum to individual uroplakins Ia, Ib, II and IIIa, and mouse monoclonal antibody AU1 against UPIIIa, have been described (Liang *et al.*, 2001). The rat monoclonal antibody 2E5 to dog MAL was also previously described (Puertollano *et al.*, 1999). Other antibodies included the following: mouse monoclonal antibody to keratin K5 and goat anti-MAL (Santa Cruz Biotechnology, Santa Cruz, CA), mouse anti–E-cadherin and rat anti–ZO-1 (Developmental Studies Hybridoma Bank, University of Iowa, Iowa City, IA), mouse monoclonal antibody to EEA1 and GM 130 (BD Bioscience, San Jose, CA), mouse monoclonal antibody to influenza hemagglutinin (kindly provided by David Sabatini, New York University School of Medicine, New York, NY), and mouse monoclonal antibody to gp135 (kindly provided by G. Ojakian, State University of New York Downstate Medical Center, Brooklyn, NY). All mouse tissues were harvested from adult mice 8–16 wk old.

Uroplakin purification

Urothelium scraped from female Swiss Webster mice (8–12 wk) was homogenized in buffer A (10 mM 4-(2-hydroxyethyl)-1-piperazineethanesulfonic acid, pH 7.5; 1 mM EDTA; 1 mM ethylene glycol tetraacetic acid; 1 mM phenylmethylsulfonyl fluoride), loaded onto a 1.6 M sucrose cushion in the same buffer, and centrifuged at 16,000 rpm for 25 min at 4°C in a Beckman Instruments (Palo Alto, CA) SW28 rotor. The crude membranes concentrated at the interface were isolated, washed with buffer A, treated with 2% Sarkosyl in buffer A for 10 min at 25°C, and pelleted, resulting in the Sarkosyl-insoluble urothelial plaques (asymmetric unit membranes [AUMs]; Wu *et al.*, 1994; Liang *et al.*, 2001; Zhou *et al.*, 2001).

Deglycosylation and immunoblotting

For endoglycosidase H (Endo H) digestion, urothelial AUM proteins were denatured in 0.5% SDS and 1% β-mercaptoethanol at 25°C for 10 min, made to contain 50 mM sodium citrate (pH 5.5), and incubated with Endo H at 37°C for 1 h (complete deglycosylation) per manufacturer's instructions (New England BioLabs, Beverly, MA). For Endo F digestion, sodium phosphate (pH 7.5) and NP-40 were added to the denatured proteins to a final concentration of 50 mM and 1%, respectively, and the mixture was incubated with Endo F. SDS–PAGE and immunoblotting were done as described (Liang *et al.*, 2001). Briefly, samples were subjected to SDS–PAGE in 17% acrylamide gels under reducing conditions and transferred to nitrocellulose membranes. After blocking with 5% nonfat dry milk and 0.05% Tween 20 in phosphate-buffered saline (PBS), blots were incubated with the primary antibody, washed, incubated for 1 h with goat anti–mouse or anti–rat immunoglobulin G (IgG) antibodies coupled to horseradish peroxidase, washed extensively, and developed using an enhanced chemiluminescence Western blotting kit (Amersham Pharmacia Biotech, Uppsala, Sweden).

N-terminal protein sequencing

Proteins separated by SDS–PAGE were transferred onto a polyvinylidene fluoride membrane and stained with Coomassie brilliant blue for 1 min. After destaining in 50% methanol and extensive washing in water, protein bands were excised and cut into small pieces. Amino-terminal sequencing was carried out by Edman degradation on a pulsed-liquid-phase sequencer, model 477 A (Applied Biosystems, Foster City, CA).

RNA purification and cDNA cloning

Total RNA was isolated according to Chomczynski and Sacchi (1987). cDNA was synthesized from 1 pg of total RNA using 200 U of Moloney murine leukemia virus reverse transcriptase in 10 mM dithiothreitol, 1 mM deoxynucleotide triphosphates each, 160 U of RNase inhibitor, and 1.6 pg of random primers in 20 µl of a buffer containing 50 mM Tris-HCl, pH 8.3, 75 mM KCl, and 3 mM $MgCl_2$. Extension was allowed to occur for 30 min at 42°C and stopped by heating for 5 min at 94°C. PCR amplification was performed in the

same tube by addition of 0.5 U of Taq DNA polymerase and 10 pmol of the primers. The full-length cDNAs of mouse uroplakins and MAL cDNA were obtained from mouse bladder total RNA by RT-PCR and subcloned into the pCDNA3 vector, and the constructs were verified by sequencing. The correct plasmids were amplified in bacteria strain Top10 and purified with Maxi Prep Kit (Qiagen, Valencia, CA).

Biotinylation of mouse urothelial surface

Female Swiss Webster mice (8–12 wk) were anesthetized under 2% isoflurane in oxygen, catheterized using a PE10 polyethylene tubing, and their bladders washed with PBS. Seventy-five microliters of sulfo–*N*-hydroxysuccinimide (NHS)-LC-biotin solution in PBS (1 mg/ml) were injected into bladder lumen over a course of 5 min. After 15 min, the bladder was rinsed with 75 µl of PBS and immediately injected with 75 µl of 50 mM lysine solution in PBS, which was left in the bladder for 15 min to quench the biotinylation reaction. Finally, the bladder was rinsed with PBS and fixed in situ with 75 µl of 10% formalin/PBS and sectioned, and the biotin was visualized using fluorescein isothiocyanate (FITC)–conjugated streptavidin (green fluorescence; nuclei counterstained in blue with 4′,6-diamidino-2-phenylindole).

Cell culture, transfection, and immunofluorescence staining

MDCK cells (strain II; American Type Culture Collection, Manassas, VA) were cultured in DMEM (Life Technologies, Rockville, MD) containing 15% fetal bovine serum (HyClone Laboratories, Logan, UT), penicillin (100 U/ml), and streptomycin (100 µg/ml) in a 5% CO_2 atmosphere. When grown on filters, 2×10^5 cells were seeded on polycarbonate membranes (diameter, 0.4 µm pore size; Transwell chambers; Costar, Cambridge, MA). The plasmids containing cDNA or siRNA were transfected using Nucleofector per protocols from Amaxa Biosystems (Gaithersburg, MD). Three separate filters were used for each condition, and the mean of transepithelial resistance (TER; ohms/cm^2) was calculated after background subtraction. Cells grown on coverslips or Transwell filters, or tissue sections, were fixed and used for indirect immunofluorescence staining. Primary antibodies in 3% bovine serum albumin were incubated with samples for 1 h at 25°C, followed by incubating with a secondary antibody (Alexa 488–conjugated donkey anti–mouse or Alexa 594 donkey anti–rabbit IgG). Images were collected using an Axioskop 2 fluorescence microscope with AxioVision 4.5 software (Carl Zeiss, Jena Germany).

Electron microscopy

For transmission electron microscopy, mouse bladders were cut into small pieces (<1 mm^2), fixed with 2.5% glutaraldehyde in 0.1 M sodium cacodylate buffer (pH 7.4), postfixed with 1% (wt/vol) osmium tetroxide, and embedded in EMbed 812 (Electron Microscopy Sciences, Hatfield, PA) as described (Liang *et al.*, 2001). For immuno–electron microscopy, mouse bladders were fixed for 4 h at 4°C in a freshly prepared solution containing 3% paraformaldehyde, 0.1% glutaraldehyde, and 4% sucrose. A 0.1 M sodium cacodylate buffer (pH 7.4) was used for LK4M embedment, and 0.1 M PBS (pH 7.4) was used as buffer for cryoimmunolabeling. Goat anti–mouse IgG conjugated with 10- or 15-nm gold particles (Amersham Life Science, Arlington Heights, IL), Nanogold conjugated anti–goat Fab′, and HQ silver enhancement kit (Nanoprobes, Yaphank, NY) were used for antigen detection (Liang *et al.*, 2001; Romih *et al.*, 2005). Stained grids were examined using a Philips CM-12 electron microscope (FEI, Eindhoven, Netherlands) and photographed with a Gatan (4k × 2.7k) digital camera (Gatan, Pleasanton, CA).

siRNA

MAL siRNA and control sequences were designed based on the algorism variable at https://rnaidesigner.invitrogen.com/rnaiexpress/rnaiExpress.jsp?cid=fl-RNAIEXPRESS. Three candidate double-stranded stealth RNA targeting dog MAL were designed and synthesized by Invitrogen: si200 (5′-CAG CCC UGC UUG UCC UGU ACA UAA U-3′), si269 (5′-CCU ACC ACU GUA UUG CUG CCC UGU U-3′), and si411 (5′-GCU GUA CGU GGU CCA UGC AGU GUU U -3′), plus a control scrambled sequence (5′-CCU UCA CUA UGU CGU CCC GUC AGU U-3′). The efficiency of MAL knockdown was measured by Western blot with monoclonal antibody anti-MAL 2E5 (Supplemental Figure S3).

Domain-selective apical biotinylation and affinity purification

MDCK cells were seeded at confluent levels on 24-mm polyester tissue culture inserts (0.4-µm pore size; Transwell). TER (ohms/cm^2) was monitored using EVOM (WPI, Sarasota, FL), and an empty filter was used as a control for background resistance. For detecting membrane proteins newly exposed on the apical surface, the apical surface of the cells was washed with ice-cold PBS containing 0.1 mM $CaCl_2$ and 1 mM $MgCl_2$ and treated for 30 min with ice-cold PBS containing 2 mM sulfo-SHPP, 0.1 mM $CaCl_2$, and 1 mM $MgCl_2$. After incubation at 37°C for 6 h, cells were washed with ice-cold PBS containing 0.1 mM $CaCl_2$ and 1 mM $MgCl_2$ and treated with a PBS solution containing sulfo-NHS-biotin (0.5 mg/ml). After 30 min at 4°C, the solution was removed and remaining unreacted biotin was quenched by incubation with ice-cold, serum-free DME. Apically labeled monolayers were finally washed with PBS and extracted with 0.5 ml of a buffer containing 25 mM Tris-HCl (pH 7.5), 150 mM NaCl, 5 mM EDTA, 1% Triton X-100, and 60 mM octyl-glucoside containing protease inhibitors. Cell lysate was incubated with streptavidin beads and rotated overnight at 4°C. The bead-bound proteins were analyzed by SDS–PAGE, and the apical proteins were detected by Western blot with appropriate antibodies.

Lipid raft assay

Total membrane proteins from the urothelia scraped from 10 mouse bladders were suspended in 1.8 ml of 20 mM Tris-HCl, pH 7.5, 20 mM NaCl, 1 mM EDTA containing 55% sucrose, and 0.5% Triton X-100 at 4°C for 30 min. The lysate was brought to a final volume of 2 ml and placed at the bottom of a SW41 centrifuge tube, followed by 7 ml of 37% and 2 ml of 5% sucrose layers. After centrifugation at 39,000 rpm at 4°C for 18 h in a SW41 rotor (Beckman Instruments), 11× 1-ml fractions were collected from the bottom of the tube, and the proteins of each fractions were analyzed by SDS–PAGE and subjected to silver staining and immunoblotting.

ACKNOWLEDGMENTS

We thank Xiangpeng Kong, Melanie Pearson, Angel Pellicer, David Sabatini, and Xue-Ru Wu for stimulating discussions and NYULMC Microscopy Core for electron microscopy services. This work was supported by National Institutes of Health Grants DK52206 (T.T.S. and G.K.) and DK39753 (T.T.S.), the NYU Center of Excellence for Urological Diseases and Selander Foundation, Swiss National Science Foundation Grant 31003A-12510 (N.S.-W.), the Spanish Ministerio de Ciencia e Innovación (CTQ2010-18644 [J.L.L.-G.], BFU2009-07886 [M.A.A.]), and Consolider COAT CSD2009-00016 (M.A.A.). J.L.L.-G. was supported by the Ramón y Cajal program from the Spanish Ministerio de Cienca e Innovación.

REFERENCES

Alonso MA, Weissman SM (1987). cDNA cloning and sequence of MAL, a hydrophobic protein associated with human T-cell differentiation. Proc Natl Acad Sci USA 84, 1997–2001.

Amano O, Kataoka S, Yamamoto TY (1991). Turnover of asymmetric unit membranes in the transitional epithelial superficial cells of the rat urinary bladder. Anat Rec 229, 9–15.

Back N, Rajagopal C, Mains RE, Eipper BA (2010). Secretory granule membrane protein recycles through multivesicular bodies. Traffic 11, 972–986.

Carmosino M, Rizzo F, Procino G, Basco D, Valenti G, Forbush B, Schaeren-Wiemers N, Caplan MJ, Svelto M (2010a). MAL/VIP17, a new player in the regulation of NKCC2 in the kidney. Mol Biol Cell 21, 3985–3997.

Carmosino M, Valenti G, Caplan M, Svelto M (2010b). traffic towards the cell surface: how to find the route. Biol Cell 102, 75–91.

Chen Y, Guo X, Deng FM, Liang FX, Sun W, Ren M, Izumi T, Sabatini DD, Sun TT, Kreibich G (2003). Rab27b is associated with fusiform vesicles and may be involved in targeting uroplakins to urothelial apical membranes. Proc Natl Acad Sci USA 100, 14012–14017.

Cheong KH, Zacchetti D, Schneeberger EE, Simons K (1999). VIP17/MAL, a lipid raft-associated protein, is involved in apical transport in MDCK cells. Proc Natl Acad Sci USA 96, 6241–6248.

Chomczynski P, Sacchi N (1987). Single-step method of RNA isolation by acid guanidinium thiocyanate-phenol-chloroform extraction. Anal Biochem 162, 156–159.

Coskun U, Simons K (2010). Membrane rafting: from apical sorting to phase segregation. FEBS Lett 584, 1685–1693.

Duncan MJ, Li G, Shin JS, Carson JL, Abraham SN (2004). Bacterial penetration of bladder epithelium through lipid rafts. J Biol Chem 279, 18944–18951.

Estrada B, Maeland AD, Gisselbrecht SS, Bloor JW, Brown NH, Michelson AM (2007). The MARVEL domain protein, Singles Bar, is required for progression past the pre-fusion complex stage of myoblast fusion. Dev Biol 307, 328–339.

Folsch H, Mattila PE, Weisz OA (2009). Taking the scenic route: biosynthetic traffic to the plasma membrane in polarized epithelial cells. Traffic 10, 972–981.

Frank M, Atanasoski S, Sancho S, Magyar JP, Rulicke T, Schwab ME, Suter U (2000). Progressive segregation of unmyelinated axons in peripheral nerves, myelin alterations in the CNS, and cyst formation in the kidneys of myelin and lymphocyte protein-overexpressing mice. J Neurochem 75, 1927–1939.

Frank M, van der Haar ME, Schaeren-Wiemers N, Schwab ME (1998). rMAL is a glycosphingolipid-associated protein of myelin and apical membranes of epithelial cells in kidney and stomach. J Neurosci 18, 4901–4913.

Fullekrug J, Simons K (2004). Lipid rafts and apical membrane traffic. Ann NY Acad Sci 1014, 164–169.

Gundelfinger ED, Kessels MM, Qualmann B (2003). Temporal and spatial coordination of exocytosis and endocytosis. Nat Rev Mol Cell Biol 4, 127–139.

Hemler ME (2003). Tetraspanin proteins mediate cellular penetration, invasion, and fusion events and define a novel type of membrane microdomain. Annu Rev Cell Dev Biol 19, 397–422.

Hicks RM (1975). The mammalian urinary bladder: an accommodating organ. Biol Rev Camb Philos Soc 50, 215–246.

Hicks RM, Ketterer B (1969). Hexagonal lattice of subunits in the thick luminal membrane of the rat urinary bladder. Nature 224, 1304–1305.

Hu CC, Bachmann T, Zhou G, Liang FX, Ghiso J, Kreibich G, Sun TT (2008). Assembly of a membrane receptor complex: roles of the uroplakin II prosequence in regulating uroplakin bacterial receptor oligomerization. Biochem J 414, 195–203.

Hu CC, Liang FX, Zhou G, Tu L, Tang CH, Zhou J, Kreibich G, Sun TT (2005). Assembly of urothelial plaques: tetraspanin function in membrane protein trafficking. Mol Biol Cell 16, 3937–3950.

Hu P, Deng FM, Liang FX, Hu CM, Auerbach AB, Shapiro E, Wu XR, Kachar B, Sun TT (2000). Ablation of uroplakin III gene results in small urothelial plaques, urothelial leakage, and vesicoureteral reflux. J Cell Biol 151, 961–972.

Hu P, Meyers S, Liang FX, Deng FM, Kachar B, Zeidel ML, Sun TT (2002). Role of membrane proteins in permeability barrier function: uroplakin ablation elevates urothelial permeability. Am J Physiol Renal Physiol 283, F1200–1207.

Hudoklin S, Jezernik K, Neumuller J, Pavelka M, Romih R (2011). Urothelial plaque formation in post-Golgi compartments. PLoS One 6, e23636.

Jacobson K, Mouritsen OG, Anderson RG (2007). Lipid rafts: at a crossroad between cell biology and physics. Nat Cell Biol 9, 7–14.

Kachar B, Liang F, Lins U, Ding M, Wu XR, Stoffler D, Aebi U, Sun T-T (1999). Three-dimensional analysis of the 16 nm urothelial plaque particle: luminal surface exposure, preferential head-to-head interaction, and hinge formation. J Mol Biol 285, 595–608.

Khandelwal P, Abraham SN, Apodaca G (2009). Cell biology and physiology of the uroepithelium. Am J Physiol Renal Physiol 297, F1477–F1501.

Khandelwal P, Ruiz WG, Apodaca G (2010). Compensatory endocytosis in bladder umbrella cells occurs through an integrin-regulated and RhoA- and dynamin-dependent pathway. EMBO J 29, 1961–1975.

Khandelwal P, Ruiz WG, Balestreire-Hawryluk E, Weisz OA, Goldenring JR, Apodaca G (2008). Rab11a-dependent exocytosis of discoidal/fusiform vesicles in bladder umbrella cells. Proc Natl Acad Sci USA 105, 15773–15778.

Kong XT *et al.* (2004). Roles of uroplakins in plaque formation, umbrella cell enlargement, and urinary tract diseases. J Cell Biol 167, 1195–1204.

Lazo PA (2007). Functional implications of tetraspanin proteins in cancer biology. Cancer Sci 98, 1666–1677.

Le Naour F, Andre M, Boucheix C, Rubinstein E (2006). Membrane microdomains and proteomics: lessons from tetraspanin microdomains and comparison with lipid rafts. Proteomics 6, 6447–6454.

Lewis SA, de Moura JL (1982). Incorporation of cytoplasmic vesicles into apical membrane of mammalian urinary bladder epithelium. Nature 297, 685–688.

Liang F, Kachar B, Ding M, Zhai Z, Wu XR, Sun T-T (1999). Urothelial hinge as a highly specialized membrane: detergent-insolubility, urohingin association, and in vitro formation. Differentiation 65, 59–69.

Liang FX, Riedel I, Deng FM, Zhou G, Xu C, Wu XR, Kong XP, Moll R, Sun TT (2001). Organization of uroplakin subunits: transmembrane topology, pair formation and plaque composition. Biochem J 355, 13–18.

Liebert M, Hubbel A, Chung M, Wedemeyer G, Lomax MI, Hegeman A, Yuan TY, Brozovich M, Wheelock MJ, Grossman HB (1997). Expression of mal is associated with urothelial differentiation in vitro: identification by differential display reverse-transcriptase polymerase chain reaction. Differentiation 61, 177–185.

Lin JH, Wu XR, Kreibich G, Sun TT (1994). Precursor sequence, processing, and urothelium-specific expression of a major 15-kDa protein subunit of asymmetric unit membrane. J Biol Chem 269, 1775–1784.

Lingwood D, Simons K (2010). Lipid rafts as a membrane-organizing principle. Science 327, 46–50.

Magal LG, Yaffe Y, Shepshelovich J, Aranda JF, de Marco Mdel C, Gaus K, Alonso MA, Hirschberg K (2009). Clustering and lateral concentration of raft lipids by the MAL protein. Mol Biol Cell 20, 3751–3762.

Marazuela M, Acevedo A, Adrados M, Garcia-Lopez MA, Alonso MA (2003). Expression of MAL, an integral protein component of the machinery for raft-mediated pical transport, in human epithelia. J Histochem Cytochem 51, 665–674.

Martin-Belmonte F, Arvan P, Alonso MA (2001). MAL mediates apical transport of secretory proteins in polarized epithelial Madin-Darby canine kidney cells. J Biol Chem 276, 49337–49342.

Martin-Belmonte F, Kremer L, Albar JP, Marazuela M, Alonso MA (1998). Expression of the MAL gene in the thyroid: the MAL proteolipid, a component of glycolipid-enriched membranes, is apically distributed in thyroid follicles. Endocrinology 139, 2077–2084.

Martin-Belmonte F, Puertollano R, Millan J, Alonso MA (2000). The MAL proteolipid is necessary for the overall apical delivery of membrane proteins in the polarized epithelial Madin-Darby canine kidney and Fischer rat thyroid cell lines. Mol Biol Cell 11, 2033–2045.

Mellman I, Nelson WJ (2008). Coordinated protein sorting, targeting and distribution in polarized cells. Nat Rev. Mol Cell Biol 9, 833–845.

Min G, Wang H, Sun TT, Kong XP (2006). Structural basis for tetraspanin functions as revealed by the cryo-EM structure of uroplakin complexes at 6-A resolution. J Cell Biol 173, 975–983.

Min G, Zhou G, Schapira M, Sun TT, Kong XP (2003). Structural basis of urothelial permeability barrier function as revealed by cryo-EM studies of the 16 nm uroplakin particle. J Cell Sci 116, 4087–4094.

Negrete HO, Lavelle JP, Berg J, Lewis SA, Zeidel ML (1996). Permeability properties of the intact mammalian bladder epithelium. Am J Physiol 271, F886–F894.

Paladino S, Sarnataro D, Pillich R, Tivodar S, Nitsch L, Zurzolo C (2004). Protein oligomerization modulates raft partitioning and apical sorting of GPI-anchored proteins. J Cell Biol 167, 699–709.
Paladino S, Sarnataro D, Tivodar S, Zurzolo C (2007). Oligomerization is a specific requirement for apical sorting of glycosyl-phosphatidylinositol-anchored proteins but not for non-raft-associated apical proteins. Traffic 8, 251–258.
Puertollano R, Alonso MA (1999). MAL, an integral element of the apical sorting machinery, is an itinerant protein that cycles between the *trans*-Golgi network and the plasma membrane. Mol Biol Cell 10, 3435–3447.
Puertollano R, Martin-Belmonte F, Millan J, de Marco MC, Albar JP, Kremer L, Alonso MA (1999). The MAL proteolipid is necessary for normal apical transport and accurate sorting of the influenza virus hemagglutinin in Madin-Darby canine kidney cells. J Cell Biol 145, 141–151.
Rodriguez-Boulan E, Kreitzer G, Musch A (2005). Organization of vesicular trafficking in epithelia. Nat Rev Mol Cell Biol 6, 233–247.
Romih R, Korosec P, de Mello W Jr, Jezernik K (2005). Differentiation of epithelial cells in the urinary tract. Cell Tissue Res 320, 259–268.
Sanchez-Pulido L, Martin-Belmonte F, Valencia A, Alonso MA (2002). MARVEL: a conserved domain involved in membrane apposition events. Trends Biochem Sci 27, 599–601.
Schaeren-Wiemers N, Bonnet A, Erb M, Erne B, Bartsch U, Kern F, Mantei N, Sherman D, Suter U (2004). The raft-associated protein MAL is required for maintenance of proper axon–glia interactions in the central nervous system. J Cell Biol 166, 731–742.
Schaeren-Wiemers N, Valenzuela DM, Frank M, Schwab ME (1995). Characterization of a rat gene, rMAL, encoding a protein with four hydrophobic domains in central and peripheral myelin. J Neurosci 15, 5753–5764.
Severs NJ, Hicks RM (1979). Analysis of membrane structure in the transitional epithelium of rat urinary bladder. 2. The discoidal vesicles and Golgi apparatus their role in luminal membrane biogenesis. J Ultrastruct Res 69, 279–296.
Simons K, Gerl MJ (2010). Revitalizing membrane rafts: new tools and insights. Nat Rev. Mol Cell Biol 11, 688–699.
Sudhof TC, Rothman JE (2009). Membrane fusion: grappling with SNARE and SM proteins. Science 323, 474–477.
Tall RD, Alonso MA, Roth MG (2003). Features of influenza HA required for apical sorting differ from those required for association with DRMs or MAL. Traffic 4, 838–849.
Thumbikat P, Berry RE, Zhou G, Billips BK, Yaggie RE, Zaichuk T, Sun TT, Schaeffer AJ, Klumpp DJ (2009). Bacteria-induced uroplakin signaling mediates bladder response to infection. PLoS Pathog 5, e1000415.
Truschel ST, Wang E, Ruiz WG, Leung SM, Rojas R, Lavelle J, Zeidel M, Stoffer D, Apodaca G (2002). Stretch-regulated exocytosis/endocytosis in bladder umbrella cells. Mol Biol Cell 13, 830–846.
Tu L, Sun TT, Kreibich G (2002). Specific heterodimer formation is a prerequisite for uroplakins to exit from the endoplasmic reticulum. Mol Biol Cell 13, 4221–4230.
Vagin O, Kraut JA, Sachs G (2009). Role of N-glycosylation in trafficking of apical membrane proteins in epithelia. Am J Physiol Renal Physiol 296, F459–F469.
Vergara JA, Longley W, Robertson JD (1969). A hexagonal arrangement of subunits in membrane of mouse urinary bladder. J Mol Biol 46, 593–596.
Vogel SS (2009). Channeling calcium: a shared mechanism for exocytosis-endocytosis coupling. Sci Signal 2, pe80.
Wang H, Min G, Glockshuber R, Sun TT, Kong XP (2009). Uropathogenic *E. coli* adhesin-induced host cell receptor conformational changes: implications in transmembrane signaling transduction. J Mol Biol 392, 352–361.
Wright MD, Moseley GW, van Spriel AB (2004). Tetraspanin microdomains in immune cell signalling and malignant disease. Tissue Antigens 64, 533–542.
Wu XR, Kong XP, Pellicer A, Kreibich G, Sun TT (2009). Uroplakins in urothelial biology, function, and disease. Kidney Int 75, 1153–1165.
Wu XR, Lin JH, Walz T, Haner M, Yu J, Aebi U, Sun TT (1994). Mammalian uroplakins. A group of highly conserved urothelial differentiation-related membrane proteins. J Biol Chem 269, 13716–13724.
Wu XR, Manabe M, Yu J, Sun TT (1990). Large scale purification and immunolocalization of bovine uroplakins I, II, and III. Molecular markers of urothelial differentiation. J Biol Chem 265, 19170–19179.
Wu XR, Sun TT (1993). Molecular cloning of a 47 kDa tissue-specific and differentiation-dependent urothelial cell surface glycoprotein. J Cell Sci 106, 31–43.
Wu XR, Sun TT, Medina JJ (1996). In vitro binding of type 1-fimbriated *Escherichia coli* to uroplakins Ia and Ib: relation to urinary tract infections. Proc Natl Acad Sci USA 93, 9630–9635.
Yanez-Mo M, Barreiro O, Gordon-Alonso M, Sala-Valdes M, Sanchez-Madrid F (2009). Tetraspanin-enriched microdomains: a functional unit in cell plasma membranes. Trends Cell Biol 19, 434–446.
Yu J, Lin JH, Wu XR, Sun TT (1994). Uroplakins Ia and Ib, two major differentiation products of bladder epithelium, belong to a family of four transmembrane domain (4TM) proteins. J Cell Biol 125, 171–182.
Zacchetti D, Peranen J, Murata M, Fiedler K, Simons K (1995). VIP17/MAL, a proteolipid in apical transport vesicles. FEBS Lett 377, 465–469.
Zhou G, Mo WJ, Sebbel P, Min G, Neubert TA, Glockshuber R, Wu XR, Sun TT, Kong XP (2001). Uroplakin Ia is the urothelial receptor for uropathogenic *Escherichia coli*: evidence from in vitro FimH binding. J Cell Sci 114, 4095–4103.